ESTIMATING INTRINSIC ATTENUATION FROM SEISMIC INTERFEROMETRY AND TIME REVERSAL

by

Conrad M. Newton, IV

A thesis submitted to the Faculty and the Board of Trustees of the Colorado School of Mines in partial fulfillment of the requirements for the degree of Master of Science (Geophysics).

Golden, Colorado

Date _____

Signed: _____
Conrad M. Newton, IV

Signed: _____
Dr. Roelof K. Snieder
Thesis Advisor

Golden, Colorado

Date _____

Signed: _____
Dr. Terence K. Young
Professor and Head
Department of Geophysics

ABSTRACT

Seismic wave fields used in imaging the subsurface are often assumed to be the response of elastic media that do not dissipate mechanical energy into heat. To accurately describe the Earth's response to seismic sources, however, anelastic effects must be included. Geophysicists incorporate intrinsic attenuation, characterized by the quality factor Q, to generate enhanced images with correct amplitudes, discern fluid types and saturation percentages of reservoirs in situ, and use attenuation as an indicator of structural deterioration to civil structures. In my thesis, I discuss monitoring civil structures fitted with instruments to estimate intrinsic attenuation.

Structural engineers have measured a building's response to strong motion from civil structures that have been instrumented with accelerometers, such as the Robert A. Millikan Library of the California Institute of Technology. The attenuation of the motion of this building has been measured using seismic interferometry techniques in the past. We use the breaking of the temporal symmetry of the wave equation by attenuation, in combination with seismic interferometry, to estimate attenuation. These estimates are made from fitting the differences in acausal and causal wave forms obtained from different deconvolution processes. We apply deconvolution interferometry to the motion recorded at the Millikan Library and obtain estimates of intrinsic attenuation that compare well to past measurements. This technique has more precision for higher frequencies than earlier measurements that are based on seismic interferometry, and it is not dependent on radiation losses at the base of the building.

Chapter 1 of my thesis gives an introduction to discuss the importance of measuring intrinsic attenuation and the effects of attenuation concerning time reversal. In Chapter 2 I discuss time-reversal symmetry and the role time-reversal symmetry plays

in geophysical data processing. Chapter 3 describes the newly proposed method in detail to discuss the advantages over past methods of acquiring attenuation estimates in civil structures and the limitations of this method. I discuss Gabor deconvolution as being an extension of the proposed method of deconvolution interferometry with time reversal by performing the fitting procedure in the time-frequency domain in Chapter 4. I conclude with a brief description of future work for the proposed method of using deconvolution interferometry with time reversal.

TABLE OF CONTENTS

LIST OF FIGURES AND TABLES

LIST OF ABBREVIATIONS

single degree of freedom	SDOF
seismic interferometry	SI
time reversal	TR
time reversal invariance	TRI

ACKNOWLEDGMENTS

I began working on attenuation estimation in the Summer of 2010 under Dr. Roel Snieder after being asked to join the Center for Wave Phenomena as a research assistant. Dr. Snieder enhanced my graduate career by extending a research position to me as I was currently seeking a Master of Engineering with no research. His thoughtful acts of guidance is the reason I have arrived to the position I am currently. I am proud to think of him as more than an advisor but also as a friend.

I would also like to thank the Center for Wave Phenomena consortium for funding my research and exposing me to new ideas. I also want to thank my research committee members Dr. Mike Batzle and Dr. Walt Lynn for their support, help, and guidance on my project. Their insight extended my work outside the intent of the application. I also want to thank the CWP faculty, especially Dr. Dave Hale for his teachings on signal processing and ideas for research. Dr. Paul Sava for his charming demeanor around the office that helps keep graduate students jovial. Dr. Ilya Tsvankin for his sincere understanding.

I have been fortunate to be surrounded by intelligent and caring colleagues in the Geophysics Department. I would especially like to thank Bharath Shekar for his insightful discussions and being my comrade around the office and Clement Fleury for his trouble-shooting abilities, insight on my topic, and a comrade.

I also want to thank my family for always supporting me and giving me encouragement. They were the driving force for me to complete my work here as a student of the Colorado School of Mines. Thank you all.

To my family and friends

CHAPTER 1

INTRODUCTION

Geophysicists of today work to determine the structure and properties of the interior of the Earth for exploration of hydrocarbon, water, and mineral resources. This work is also extended to include risk and hazard assessment, geotechnical construction, planetary geophysics, atmospheric science, defense projects, and debris flows. Processing geophysicists create models that accurately describe the Earth system under investigation through various remote sensing techniques. These techniques yield data that can be mathematically linked to models that describe relevant properties of the subsurface of Earth (Tarantola, 2005). Geophysicists also collect potential field data like gravity, magnetic, electric and electromagnetic field data and seismic data such as surface seismic (P- and S-waves), sonic logs, and vertical seismic profiles for hydrocarbon and mineral resource exploration and water resource exploration (Telford et al., 1976).

Modern geophysical data are most commonly in a digital format, and such digital data are processed to infer accurate models of the Earth. The signal convolution model, equation 1.1 below, is used to describe n elements of a data array $u[n]$ to be the convolution of a source signal $w[n]$ with the impulse response of the Earth $h[n]$ (Robinson, 1999). If the source wavelet is known, the impulse response function for the Earth gives all the information needed by geophysicists to reconstruct wave field propagation to an accurate model of Earth's subsurface. The convolution model

$$u[n] = w[n] * h[n] \tag{1.1}$$

is the ideal description of 1D (i.e. no spatial variation) recorded time signals. There is, of course, additive noise present in the signals, attenuation of signal with propagation, and other sources of error. Geophysicists eliminate as much noise as possible by the

application of signal processing techniques to increase the signal to noise ratio of the recorded data.

Data collected for geophysical applications are typically recorded from energy injected into the Earth which usually propagates in the form of waves. Wave propagation often satisfies time reversal symmetry. Simply put, data recorded at the surface of Earth can be collected, time reversed, and used to recreate wave fields propagating backwards into the Earth. This is, for example, valuable for seismic imaging where waves back propagated by this procedure are correlated with synthetic data generated from velocity models of the Earth's.

Time reversal (TR) is a property of the elastic and electromagnetic wave equations used to focus energy back to the initial time and exact location of source injection. This symmetry can be broken by factors such as flow in the medium, rotation of the medium, and dissipation of mechanical energy into heat (Fink, 2006). I focus on intrinsic attenuation because it is most relevant for geophysical applications. Intrinsic attenuation can be troublesome for applications such as imaging, but it is a necessary phenomena to characterize damping in civil structures after excitation by earthquakes. Attenuation is of particular importance for the ability of buildings to withstand earthquakes, because it is the balance of energy injected into the buildings by prolonged shaking and attenuation that determines the amplitudes of the oscillation of buildings.

Attenuation is a broad term to describe the dissipation of the mechanical or electromagnetic energy. The source energy dissipates with increased distance from the source location through spherical divergence, scattering of energy from heterogeneities, transmission and radiation losses, and energy conversion to heat called intrinsic attenuation (Gautam, 2003). Intrinsic attenuation is measured by the unitless quality factor Q that is related to the viscous damping coefficient $\zeta = 1/2Q$ most commonly used by structural engineers (Kohler et al., 2007).

Signal attenuation is prevalent in recorded wave propagation data. This poses challenges and limitations to seismic imaging. Geophysicists use elastic and electromagnetic wave propagation theory to probe the Earth's interior because such theories describe the relationship between their respective data and model parameters (Tarantola, 2005). Elastic stress fields underly seismic wave modeling, while electromagnetic fields govern wave propagation for field investigation of the electrical properties of the subsurface.

Attenuation of digital signals is a large contributor to low signal-to-noise ratio in data. The attenuated signals appear noisy because the amplitudes of the signal decrease and eventually fall below the noise level as the waves propagate. Attenuation is inherent in all wave propagation, and affects the signal at preferentially high frequencies (Futterman, 1962). For this reason the resolution of seismic models decrease with depth.

Geophysicists attempt to remove the imprint of attenuation effects by applying Q^{-1} filters to gain the amplitudes of attenuated time signals. To gain signals accurately, measurements of the attenuation must be made through inversion algorithms and lab measurements.

Geophysicists have studied intrinsic attenuation and the role of fluids and friction at the microscopic scale through lab experiments (Batzle et al., 2005; Behura et al., 2007; Spencer, 1979; Winkler and Nur, 1979; Winkler et al., 1979; Winkler and Nur, 1982; Wylie et al., 1962). These experiments usually operate at frequencies that are several orders of magnitude higher than frequencies used in seismic surveys due to scale in the lab versus the field (Gautam, 2003). Since the quality factor Q is frequency dependent, lab values for Q are not accurate for seismic frequencies, and estimations of attenuation have to be made using seismic data (Dasgupta and Clark, 1998).

In my thesis, I present in Chapter 3 a method to measure intrinsic attenuation in the Millikan Library of the California Institute of Technology after this building has been excited by the Yorba Linda earthquake on the 3^{rd} September, 2002. As an introduction to the concept of time reversal, I discuss in Chapter 2 the behavior of time reversal symmetry of wave propagation in elastic and electromagnetic wave fields. This will be done by showing that Newton's second law is time-reversal invariant, and by showing the elastic and electromagnetic wave equations are time-reversal invariant when considering media without flow, rotation, or intrinsic attenuation. These equations include a macroscopic description of attenuation that breaks time reversal symmetry. Chapter 3 has been accepted by the Bulletin of the Seismological Society of America for publication.[1] In Chapter 4, I discuss method for measuring intrinsic attenuation using Gabor deconvolution that has potential to be another method for estimating attenuation in a time-frequency domain. I finish with conclusions and provide ideas for future work using the methods discussed.

[1]Newton, C. and Snieder, R., Estimating intrinsic attenuation of a building using deconvolution interferometry and time reversal, Bull. Seismol. Soc. Am., in press, 2012

CHAPTER 2

TIME REVERSAL IN GEOPHYSICS

Time reversal invariance (TRI) refers to systems that share an intrinsic symmetry about time in the laws of physics. Sir Isaac Newton articulated the classical laws of motion that explain the kinematics of our universe. These laws have the property of of time reversal invariance. We may move forward or backwards in time without violating equations of motion. This property of TRI allows the back-projection of the motion of particles or waves to the original location of excitation. This property may appear trivial, but its applications make it invaluable to many scientists and engineers in optics, medical imaging, geophysics, and more.

The property of time reversal invariance describes a medium that supports recorded signals being reversed, reinjected, and focused temporally and spatially on the initial source (Anderson et al., 2008, 2011; Fink, 2006). If one can accurately describe the wave propagation through structures with numerical models, we can compare real data that propagates forward in time through these structures with synthetic data that propagates backward in time through numerical models. Claerbout (1971) first used this scheme of back propagation of data to develop seismic migration. This seismic imaging method relies on the assumption that the structures are made of media that are invariant to time reversal.

Geophysicists rely heavily on numerical modeling to render images of the subsurface. Though not all media are time reversal invariant (TRI), assumptions can be made and modeling can account for effects that break TR.

Most systems indeed break the symmetry of TR. When the medium under investigation is subject to rotation, flow, or material damping like intrinsic attenuation, the system is no longer invariant to time reversal (Fink, 2006). This chapter aims

to explain the concepts of TR in fundamental equations of motion and applying this symmetrical property to geophysical problems to render accurate models of the subsurface. I show how TRI is a consequence of classical laws of mechanics, and extend this concept to more advanced equations describing acoustic, elastic, and electromagnetic wave propagation that aid geophysicists in investigating the subsurface. I discuss the factors that break TR, and explore more deeply how intrinsic attenuation breaks TR.

2.1 Time Reversal Invariance

To better visualize TRI, we may observe Newton's 2^{nd} law. We define Newton's 2^{nd} law as a vector force $\mathbf{F}$ being the partial time derivative of the momentum $\mathbf{p}$ given by

$$\begin{aligned} \mathbf{F} = \dot{\mathbf{p}} = \frac{\partial (m\mathbf{v})}{\partial t} &= \frac{\partial m}{\partial t}(\mathbf{v}) + \frac{\partial \mathbf{v}}{\partial t}(m) \\ &= \frac{\partial m}{\partial (-t)}(-\mathbf{v}) + \frac{\partial (-\mathbf{v})}{\partial (-t)}(m). \end{aligned} \tag{2.1}$$

Here m is the mass of a point object and $\mathbf{v}$ is the velocity of the object. We observe the equation remains invariant to time reversal because the equations are the same after reversing the time t and velocity $\mathbf{v}$. The time reversal procedure would be similar to recording the motion of an object with a velocity $\mathbf{v}$ and viewing the footage in reverse. One would observe the object moving in a reverse direction with a velocity $-\mathbf{v}$ and arriving exactly where it began.

This symmetry is apparent in linear motion, but should also apply to angular motion as well. We apply TR to Newton's 2^{nd} law to an extended object with angular momentum $\mathbf{L}$ given by

$$\begin{aligned}\mathbf{r}\times\mathbf{F}=\dot{\mathbf{L}}=\frac{\partial(I\boldsymbol{\omega})}{\partial t} &= \boldsymbol{\omega}\frac{\partial I}{\partial t}+I\frac{\partial\boldsymbol{\omega}}{\partial t}\\ &= \frac{(\mathbf{r}\times\mathbf{v})}{|r|^2}\frac{\partial I}{\partial t}+I\frac{\partial}{\partial t}\frac{(\mathbf{r}\times\mathbf{v})}{|r|^2}\\ &= \frac{(\mathbf{r}\times-\mathbf{v})}{|r|^2}\frac{\partial I}{\partial(-t)}+I\frac{\partial}{\partial(-t)}\frac{(\mathbf{r}\times-\mathbf{v})}{|r|^2}.\end{aligned} \tag{2.2}$$

Here $\boldsymbol{\omega}$ is the angular velocity, r is the radial distance from the origin of the rotation to the object, and I is the moment of inertia. Again we see the equation behaves with invariance to the reversal of time. In a rotating system, such as the Earth, TR invariance is violated by the Earth's rotation. For waves propagating over a time t, the Earth's rotation is Ωt, with $\Omega = 2\pi/1day$ being the angular velocity of the Earth. For the time scale of a seismic experiment, $t \approx 10s$, this dimensionless number is equal to $\Omega t = 2\pi 10s/1day = 7.3\times10^{-4} \ll 1$, so the imprint on Earth's rotation on seismic imaging is, in practice, negligible. Ruigrok et al. (2008) considers teleseismic wave propagation, where the propagation time is much longer, and show how to incorporate the rotation of the Earth in seismic interferometry.

With TR symmetry supported by the physical laws of motion, we can use this property for applications in refocusing wave fields for imaging the subsurface and human organs and other material applications. TR symmetry is clear from the mathematics, but may not be so visually intuitive.

Time reversal symmetry can be visualized when considering the experiment of Derode et al. (1995). The experiment demonstrates how a device termed a Time Reversal Mirror can recover the initial source impulse. Figure 2.1 demonstrates a rendition of their experiment. In Figure 2.1a the medium represented by the blue block is a homogeneous medium with iron bars inserted at random to act as point scatterers. On the left side of the medium is a piezoelectric transducer that has transmitting and receiving (T/R) capabilities that injects an impulsive wavelet as the

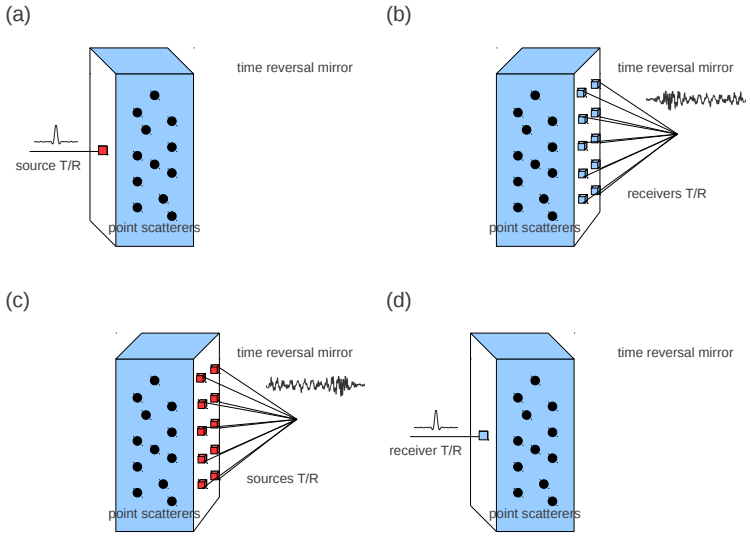

Figure 2.1: Experiment of Derode et al. (1995) with (a) piezoelectric source transducer and impulse signal, (b) piezoelectric receivers recording scattered waves, (c) receivers inject time reversed scattered waves where the receivers act as sources to refocus signal, (d) source in receiving mode records the refocused impulsive signal

source signal. Figure 2.1b shows the receiving array on the right side of the medium that makes up the time reversal mirror. These receivers record highly scattered signals that are similar to the signal adjacent to the blue block. Figure 2.1c demonstrates how the time reversal mirror reinjects a time reversed signal from the receiver locations. The piezoelectric receivers also have T/R abilities and reinject the time reversed signal with the correct synchrony to generate a complex wave field that propagates back through the medium toward the initial source. Figure 2.1d illustrates the source in receiving mode record the original impulse wavelet injected. This illustration is not accurate in that the time reversed wave field recorded at the source location in Figure 2.1d is exactly the same impulse function initially injected. In reality the signal refocused at the source location would have side lobes as artifacts to the limited aperture. To fully recover the initial impulse signal, the medium would need to have full coverage. This limits the ability of TR to refocus the source impulse without uncertainty, but the refocusing is done with enough accuracy to be used in medical

applications such as in lithotripsy where kidney stones are located and destroyed with the refocusing of ultrasonic energy and material applications where materials are coupled with a unique liquid to determine microfractures in the material (Fink, 2006).

2.2 Acoustic Wave Propagation

A linear acoustic medium does not support shear waves. Therefore, the field represented by the acoustic wave equation is comprised of only pressure waves. The homogeneous acoustic wave equation is constructed using Newton's 2^{nd} law of motion. Equation 2.3 describes how energy propagates through a liquid or gas having a real-valued compressibility. Having a complex compressibility introduces intrinsic attenuation and velocity dispersion through the Kramers-Krönig relations to satisfy causality (Futterman, 1962). Introducing the complex compressibility will break TR symmetry. The degree of attenuation needed to break TR symmetry is dependent upon the measured levels of attenuation and the duration of the signal. For example, low levels of attenuation may be considered negligible after measuring only over a few cycles, but considerable if the signal is observed over many cycles.

We may also apply the same test of TR to the acoustic wave equation as we did with Newton's 2^{nd} law.

$$\begin{aligned} \frac{1}{c^2}\frac{\partial^2 P}{\partial t^2} &= \rho\nabla\cdot\left(\frac{1}{\rho}\nabla P\right) \\ \frac{1}{c^2}\frac{\partial^2 P}{\partial\left(-t\right)^2} &= \rho\nabla\cdot\left(\frac{1}{\rho}\nabla P\right) \end{aligned} \tag{2.3}$$

$$\frac{1}{c^2}\frac{\partial^2 P}{\partial t^2} - \rho\nabla\cdot\left(\frac{1}{\rho}\nabla P\right) = \frac{1}{c^2}\frac{\partial^2 P}{\partial\left(-t\right)^2} - \rho\nabla\cdot\left(\frac{1}{\rho}\nabla P\right) \tag{2.4}$$

Here P represents the pressure field and c is the phase velocity of the fluid. This equation is TRI for small perturbations in a lossless medium. What makes this

equation invariant to time reversal is that there is no flow in the medium, the medium does not rotate, and there is no attenuation or velocity dispersion.

The acoustic wave equation allows the modeling of pressure wave fields inside an acoustic medium without losses. This makes the assumption that the medium fully restores the energy that passes through any finite element within the medium. An ideal medium as described above, however, never occurs in nature, and all media will have some losses at varying scales.

Intrinsic attenuation describes nonadiabatic media that lose some energy to heat and is characterized by the quality factor Q. There are various types of intrinsic attenuation that are dependent on the mode of wave propagation (Gautam, 2003), but I discuss the attenuation for the shear mode only.

Attenuation observations are dependent upon the dominant wavelength of the source signal. Scattering attenuation can occur in media with high levels of heterogeneities that can be sensed by the wavelength of the source signal. The heterogeneities scatter energy into multiple paths before being recorded by the instruments on the surface. The scattering may or may not significantly attenuate the signal, but scattering the energy coupled with the energy being converted to heat reduces the energy recovered by our instruments.

We may also test a visco-acoustic wave equation for TRI by including a damping term β.

$$\frac{1}{c^2}\frac{\partial^2 P}{\partial t^2} - \beta\frac{\partial P}{\partial t} = \nabla^2 P \quad (original) \tag{2.5}$$

$$\frac{1}{c^2}\frac{\partial^2 P}{\partial (-t)^2} + \beta\frac{\partial P}{\partial (-t)} = \nabla^2 P \quad (time-reversed) \tag{2.6}$$

This partial differential equation describing a visco-acoustic media is not TRI. Solutions to this wave equation describe an amplitude term to decay exponentially with increasing time after the source excitation. If the attenuation is well understood, the attenuation can be handled to correctly gain the amplitudes.

Not having a-priori knowledge of the medium's attenuation can be disastrous for structural modeling. TR techniques, however, can give qualitative and quantitative insight of the magnitude of attenuation given that there are no flows or rotations of the medium that might break the TR symmetry. To acquire such insight of the presence of attenuation would require the separation of the wave field into d'Alembert solutions that describe the direction the wave field is traveling (i.e. upgoing or downgoing wave fields) (Robinson, 1999). Successful separation of the wave fields should render symmetric time signals about time $t = 0$, but if attenuation is present the signals will have similar shape but different amplitudes. This procedure is discussed further in Chapter 3 of the thesis.

2.3 Elastic Wave Propagation

I have shown how the acoustic wave equation supports TR, and I will show how the elastic wave field also supports TR. As stated before, attenuation breaks TR symmetry of the elastic wave field. For simplicity, I will show the elastic wave equation excluding a damping term to account for the attenuation. It should be understood that including the damping term will break the TR symmetry. Elastic waves in a homogeneous isotropic medium satisfies the following differential equation (Aki and Richards, 1980)

$$(\lambda + 2\mu)\,\nabla\,(\nabla \cdot \mathbf{u}) - \mu\nabla \times \nabla \times \mathbf{u} - \rho\frac{\partial^2 \mathbf{u}}{\partial t^2} = 0. \tag{2.7}$$

Here λ and μ are Lamé material parameters, ρ is the density of the material, and $\mathbf{u}$ is the displacement vector recorded by the geophones. If we assume the material parameters λ and μ are not time variant within each medium and allow only small perturbations of the media, the equation will be TRI having only a second derivative in time of the displacement vector $\mathbf{u}$. The velocities of the medium are implicitly understood to exist in this equation as the acoustic velocity $\alpha^2 = \dfrac{\lambda + 2\mu}{\rho}$ and the shear velocity $\beta^2 = \dfrac{\mu}{\rho}$.

2.4 Electromagnetic Wave Propagation

Time reversal techniques are popular with geophysicists specialized in acoustic and elastic wave field propagation, but this property can be extended to include electromagnetic wave propagation as well. Electromagnetic energy is well suited for investigating the subsurface of the Earth for near-surface reflection responses and in situ fluid characterizations. To understand this more clearly, we look closer to the wave equation of the electric field.

To derive the homogeneous wave equation for electromagnetic wave propagation, we need to remember the following Maxwell's equations for classical electrodynamics.

$$\nabla \times \mathbf{E} = -\frac{\partial \mathbf{B}}{\partial t} \tag{2.8}$$

$$\nabla \times \mathbf{B} = \mu_0 \mathbf{J} + \mu_0 \epsilon_0 \frac{\partial \mathbf{E}}{\partial t} \tag{2.9}$$

We may start by taking the curl of the curl of the electric field $\mathbf{E}$. Recalling the vector calculus property $\nabla \times (\nabla \times \mathbf{V}) = \nabla (\nabla \cdot \mathbf{V}) - \nabla^2 \mathbf{V}$, we may write equations 2.8 and 2.9 as

$$\nabla \times (\nabla \times \mathbf{E}) = -\frac{\partial}{\partial t} \nabla \times \mathbf{B} = -\frac{\partial}{\partial t} \left(\mu_0 \mathbf{J} + \mu_0 \epsilon_0 \frac{\partial \mathbf{E}}{\partial t} \right). \tag{2.10}$$

We now make the homogeneous assumption of there being no electric source (i.e. $\nabla \cdot \mathbf{E} = 0$) and use the relation of the current density to the electric field $\mathbf{J} = \sigma \mathbf{E}$, where σ is the electrical conductivity of the material under investigation. This transforms our electromagnetic wave equation into

$$\nabla^2 \mathbf{E} = \mu_0 \sigma \frac{\partial \mathbf{E}}{\partial t} + \frac{1}{c_0^2} \frac{\partial^2 \mathbf{E}}{\partial t^2}. \tag{2.11}$$

We have included the speed of light $c_0 = \dfrac{1}{\sqrt{\mu_0 \epsilon_0}}$ in equation 2.11. We observe some similarities in the factors between the partial differential equations 2.11 and 2.5. From inspection, one may conclude that the first term on the right side of equation 2.11 is similar to the damping term in equation 2.5, and the second term on the right side of

equation 2.11 is the propagation term similar to equation 2.5. Similar to the visco-acoustic medium, without the single derivative term the wave equation is TRI. If the single derivative term contributes strongly to the wave propagation, the propagation will no longer be TRI.

We investigate the effects of these terms more closely. If we consider a complex exponential solution in the frequency domain for equation 2.11 to be $\mathbf{E} = \mathbf{E}_0 e^{i\omega t}$, we may view equation 2.11 as

$$\nabla^2 \mathbf{E} = i\omega\mu_0\sigma\mathbf{E} - \frac{\omega^2}{c_0^2}\mathbf{E}, \tag{2.12}$$

where the imaginary number $i = \sqrt{-1}$ and ω is the angular frequency. The ratio of the absolute value of the coefficients of each term can be used to understand what influences the wave propagation. The ratio of the absolute value of the first coefficient to the second coefficient is

$$\frac{\mu_0\sigma c_0^2}{\omega} = \frac{\sigma}{\omega\epsilon_0}. \tag{2.13}$$

If we hold the frequency constant, the ratio is really determined by the relationship between the electrical conductivity of the medium σ and the electrical permittivity of the medium ϵ. Note that we have changed ϵ_0 to ϵ to be more practical by considering a resisting medium instead of an ideal vacuum.

It is clear that when the medium behaves such that $\omega \gg \sigma/\epsilon$, the oscillating term will govern the propagation to behave more like seismic reflections as seen using ground penetrating radar (GPR). When $\omega \ll \sigma/\epsilon$ the medium response will be diffusive as is typical when sensing hydrocarbon fluids in situ using controlled source electromagnetic (CSEM) instruments (Constable and Srnka, 2007).

The electromagnetic wave equation behaves like the acoustic wave equation with a viscous damping term. Time reversal techniques are applicable to electromagnetic waves in media that support undamped wave propagation and are similar to methods that use acoustic waves for imaging the subsurface. When the medium breaks

the TR symmetry in geophysical applications, it is due to the damping term in the electromagnetic wave equation. This is used by exploration geophysicists to detect the presence of hydrocarbon fluids. We will look at geophysical methods that rely on the theory presented above to render information of the Earth's subsurface.

2.5 TR in Geophysical Methods

Basic wave equations that explain the propagation of information from a geophysical sources to geophysical instruments are invariant to time reversal. The TR property of wave propagation allows for modeling of the subsurface to yield models with little uncertainty. Though not all systems are TRI, as most are not, we may still be able to infer properties of the subsurface under investigation.

I will discuss geophysical methods that use acoustic, elastic, and electromagnetic wave propagation to make measurements for determining structure and properties of the subsurface. These methods rely on assumptions of both TR and the breaking of TR symmetry.

2.5.1 Acoustic and Elastic Wave Modeling

Geophysical methods that use the acoustic and elastic wave equation are referred to as seismic methods. Seismic methods are used by earthquake seismologists for determining seismic moment tensors of earthquake sources and tracking teleseismic events throughout the Earth. These methods are also used by exploration geophysicists to generate subsurface images of the Earth to locate hydrocarbon traps and for discerning fluid saturation and type in oil and gas reservoirs. Without TR imaging would not be possible.

Earthquake seismologists are faced with difficulty in survey geometry and having limited means of determining source signature and location. These surveys are called passive surveys because the seismologist do not create the seismic source. The source comes from the earthquake at an undetermined time and location. The instruments

on the surface are also much more sparse than a typical exploration survey which reduces the spatial resolution of the earthquake model. This makes the job of an earthquake seismologist much more challenging to accurately generate tomographic images and determine the earthquake source magnitude and location.

Nevertheless, earthquake seismologists use clever modeling schemes to estimate source magnitude and location by iteratively back-propagating surface data using TR and comparing it against modeled data using stratigraphic velocity models believed to accurately describe the Earth's interior. Because the spatial sampling is coarse, the velocity models are typically more broad than found in exploration surveys. There are also complications of converted shear waves and multiple reflections that every imaging geophysicist must face. The acoustic wave equation describes only pressure waves, but Earth generates both pressure and shear waves and multiple reflections generated by both wave types. If the shear waves are not used for imaging, they become noise and must be removed from the data.

Using the acoustic wave equation we can model the primary pressure wave arrivals and predict their multiple reflections. The elastic wave equation describes both pressure and shear waves, but becomes computationally costly. Using the elastic wave equation can yield more information about the subsurface material properties and anisotropy.

Exploration geophysicists have the same goal as earthquake seismologists to image the subsurface, but use a controlled source. This gives the geophysicist the luxury of knowing the location and time of excitation. There are still issues, however, of knowing and estimating the source wavelet complicated by coupling of the source to the medium, source instrument errors, and near-surface statics (Robinson, 1999). The exploration geophysicist has a survey with a finer spatial resolution than the earthquake geophysicist. This yields better resolution of the stratigraphy in the subsurface. Surveys are indeed different, but both their duty is to image the subsurface.

The imaging of the subsurface is called migration (Claerbout, 1971), and has been developed to transition from analog signals physically being migrated with pencil and compass to the digital world of supercomputing highly advanced migration algorithms to generate three dimensional images. With the advent of supercomputers, algorithms are being developed to handle the elastic wave fields that include both pressure and shear wave data. As mentioned before, the Earth is not typically TRI, and this is attributed to intrinsic attenuation in the various stratigraphic sections in the Earth. Today's migration algorithms are able to handle attenuation by applying the appropriate gain levels to the time signals before, or sometimes during, TR back propagation. Seismic inversion can model for the correct attenuation values with uncertainty. Understanding the attenuation in the time signals corresponding to the reservoir section compared to experiments done in the lab to determine intrinsic attenuation leads to what fluids are saturating the reservoir.

Time reversal is critical to the imaging process done by earthquake seismologists and exploration geophysicists. It allows for the back propagation of time signal data to be compared to modeled synthetic data to yield an accurate image. When TR symmetry is broken by attenuation, inferences can be made about fluids existing in the subsurface that are valuable to producing a hydrocarbon reservoir.

By determining intrinsic attenuation values, fluid type and saturation levels can be inferred from lab experiments. Lab experiments can determine attenuation values for dry and saturated rocks. The attenuation values indicate what fluids are present in situ. Determining the fluid content can be very difficult with surface seismic data, but repeated surveys, known as 4D seismic surveys, will indicate changes in attenuation if fluids migrate through the reservoir. The change in attenuation is due to different attenuation values associated with hydrocarbon fluids and water. Attenuation has broke the TR symmetry, but has given reservoir development information.

Changes in attenuation can indicate failure in civil structures as well (Clinton et al., 2006; Foutch, 1976; Kohler and Heaton, 2007; Kuroiwa, 1967). A select number of buildings have been fitted with seismic recording instruments to research and monitor changes over time. By breaking the TR symmetry, we can determine if these signals have been attenuated.

2.6 Summary

TR symmetry is an important property of wave propagation. It has allowed scientists to accurately image media that has been excited by wave propagation by back-propagating data compared to modeled forward synthetic data. This unique symmetry of TR can be broken by attenuation, flow, and rotation. This gives information that indicates something has broken the symmetry.

CHAPTER 3

ESTIMATING ATTENUATION OF THE MILLIKAN LIBRARY

For decades, scientists and engineers have worked to characterize building responses with the purpose of mitigating earthquake hazards and monitoring building integrity (Carder, 1936; Çelebi et al., 1993; Chopra and Naeim, 2007; Clinton et al., 2006; Foutch, 1976; Kohler and Heaton, 2007; Kuroiwa, 1967; Prieto et al., 2010; Snieder and Şafak, 2006; Trifunac, 1972). This has been done by measuring building motion, modal frequencies, intrinsic attenuation, shear velocities, and other properties. After the excitation force drives the motion of the building, intrinsic attenuation, scattering attenuation, and radiation losses dissipate the energy. Intrinsic attenuation estimates quantify the anelastic dissipation of the building's motion given by the quality factor Q or the damping coefficient ζ.

$$\zeta = \frac{1}{2Q} \tag{3.1}$$

Improving the estimation of intrinsic attenuation from the motion excited by complicated ground motion is the focus of this work. Advancing the estimation of attenuation, engineers can more accurately describe the motion of civil structures (Çelebi et al., 1993; Chopra and Naeim, 2007; Kohler et al., 2007), while geophysicists can produce more accurate models of the subsurface (Calvert, 2003) and diagnose the presence of fluids and the migration of these fluids in reservoirs (Bakulin et al., 2007).

Much has been learned from advanced instrumentation installed into buildings such as the Factor Building of UCLA and the Millikan Library of Caltech. These networks have produced large volumes of data for understanding wave propagation in buildings. Monitoring these types of buildings suggests that analysis be done over time to observe changes in the response of the building. Typically, this analysis is done for the motion excited by earthquakes (Clinton et al., 2006; Kohler et al., 2007;

Snieder and Şafak, 2006), ambient noise (Clinton et al., 2006; Derode et al., 2003; Larose et al., 2006; Prieto et al., 2010), or controlled sources (Clinton et al., 2006; Kohler and Heaton, 2007; Kuroiwa, 1967). Recently, seismic interferometry has been used for acquiring attenuation estimates (Kohler et al., 2007; Prieto et al., 2010; Snieder and Şafak, 2006).

Seismic interferometry has received much attention in the seismology community. The use of seismic interferometry has been explored for extracting Green's functions, and from this, other parameter estimations (Bakulin and Calvert, 2006; Halliday and Curtis, 2010; Snieder et al., 2006; Vasconcelos and Snieder, 2008; Wapenaar et al., 2010). Deconvolution interferometry is preferable, for reasons discussed later, for retrieving attenuation estimates. Snieder and Şafak (2006) and Kohler et al. (2007) use deconvolution interferometry for the Millikan Library and Factor Building, respectively, to acquire attenuation estimates. Our approach is similar, but we use upgoing and downgoing decomposed waves and time reversal to attain attenuation measurements.

The concept that attenuation breaks time reversal symmetry facilitates our measurements of attenuation (Fink, 2006; Gosselet and Singh, 2007). Wave field decomposition, in combination with deconvolution interferometry, generates acausal and causal wave forms (Snieder et al., 2006). Here, we define acausal to describe the wave forms occuring before time $t = 0$. We compare these wave forms, and from their differences, estimate intrinsic attenuation. Since our estimate of attenuation hinges on a comparison of causal and acausal waveforms, we obtain an estimate of intrinsic attenuation because scattering attenuation is causal and invariant for time reversal. In the following we use the term attenuation for intrinsic attenuation.

Much like the method used by Snieder and Şafak (2006), we base our estimates on a linear least-squares fit to the natural logarithm of the deconvolved wave form envelopes. We acquire accurate and precise estimates of attenuation that are fre-

quency dependent and compare well to previous attenuation estimates. Our method acquires frequency-dependent attenuation estimates that do not require any normal mode analysis and estimates are more precise than estimates taken from traveling waves.

The recorded shear waveforms were excited by the Yorba Linda earthquake and consist of two N-S and one E-W accelerations of the Millikan Library in 10 floors above the surface and a basement below the surface. Only one N-S acceleration dataset was used for this investigation (Figure 3.1). There were some instrument coupling issues in the other two datasets as well. Building dimensions and details pertaining to the structure and instrumentation can be found in many articles, but most historical and recently notable, Kuroiwa (1967) and Clinton et al. (2006). Using only the N-S motion of the building constrains our analysis to 1 degree of freedom. The geometry of the building allows for a clamped beam model to represent the motion of the structure. The Millikan Library naturally has 3 degrees of freedom in building motion, and $3n$ degrees of freedom if we consider a number of floors denoted by n (Şafak, 1999). Our purpose is to demonstrate the application of this method, but our method can be extended to include more degrees of freedom.

We first discuss the basic theory behind deconvolution interferometry and time reversal. We give an example of why deconvolution interferometry is chosen, and how the deviation from time reversal symmetry indicates the presence of attenuation and facilitates the measurement of attenuation. Next, we discuss the methodology used to achieve these results. We finish by comparing estimates of attenuation with those made from past interferometric methods of the Yorba Linda earthquake data recorded at the Millikan Library.

3.1 Theory

Seismic interferometry using deconvolution has become increasingly popular for applications in seismic imaging, parameter estimation, and passive monitoring (Curtis

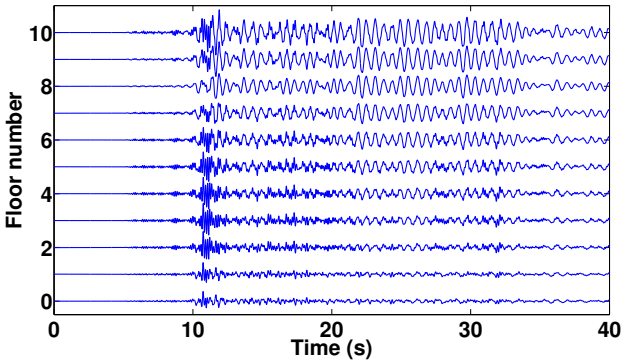

Figure 3.1: Yorba Linda earthquake data recorded at the Millikan Library, California Institute of Technology in Pasadena, California. The wave forms indicate accelerations in the N-S direction, and the floor numbers correspond to the location in the building where the data were recorded. Floor 0 is the basement floor.

et al., 2006; Kohler et al., 2007; Minato et al., 2011; Prieto et al., 2010; Snieder and Şafak, 2006; Snieder et al., 2006; Vasconcelos and Snieder, 2008). Typically cross correlation representation theorems are used to acquire the correct Green's function between receivers. Snieder (2007) shows that in the presence of dissipation, cross correlation type seismic interferometry cannot accurately determine the attenuation response between receivers unless the medium is completely covered by sources. We first briefly explore the reasons why deconvolution seismic interferometry is preferred over cross correlation seismic interferometry in estimating attenuation, especially with passive seismic data.

Consider a simple one-dimensional seismic-interferometry experiment in a homogeneous dissipative medium to illustrate my decision to use deconvolution interferometry. Consider a source located at position r_S, and receivers located at r_A and r_B, Figure 3.2. If a dissipating wave propagates away from the source and is recorded by receivers, seismic interferometry can be used to determine the response between those receivers. Seismic interferometry is a tool to measure the response between receivers, where the source position is redatumed to a known receiver location by the virtual source method (Schuster, 2009). Though the source signature of the actual

source and virtual source are indeed different, the wave state obtained from seismic interferometry obeys the same wave equation as the original system (Snieder et al., 2006), and we can determine the system response to a virtual source. Examining the deconvolution and cross correlation operations, for this example, gives insight why deconvolution is preferred for measuring attenuation. In our thought experiment, the receivers record the following frequency-domain wave fields:

Figure 3.2: Definition of geometric parameters for 1D wave propagation example

$$U(r_A,\omega) \;=\; S(r_S,\omega)\; e^{-\gamma(r_A-r_S)}\; e^{ik(r_A-r_S)} \tag{3.2}$$

$$U(r_B,\omega) \;=\; S(r_S,\omega)\; e^{-\gamma(r_B-r_S)}\; e^{ik(r_B-r_S)}, \tag{3.3}$$

where $S(r_S,\omega)$ is the source spectrum, k is the wavenumber, and γ the attenuation coefficient.

The choice of which seismic interferometric operation gives an accurate estimation of the attenuation becomes apparent from the application of each interferometric technique to the wave forms $U(r_A,\omega)$ and $U(r_B,\omega)$. Cross correlation interferometry applied to these wave fields gives, in the frequency domain,

$$\begin{aligned} CC(r_B,r_A,\omega) &= U(r_B,\omega)U^*(r_A,\omega) \\ &= |S(r_S,\omega)|^2\; e^{-\gamma(r_B+r_A-2r_S)}\; e^{ik(r_B-r_A)}. \end{aligned} \tag{3.4}$$

The phase is correct, but the amplitude is incorrect because it depends on the *sum* of the positions $r_B + r_A$ rather than the *difference* $r_B - r_A$. The amplitudes esti-

mated from cross correlation are thus incorrect for attenuation analysis. In contrast, deconvolution of the fields of equations (2) and (3) in the frequency domain gives

$$\begin{aligned} D(r_B, r_A, \omega) &= \frac{U(r_B, \omega)}{U(r_A, \omega)} \\ &= e^{-\gamma(r_B - r_A)}\ e^{ik(r_B - r_A)}. \end{aligned} \tag{3.5}$$

With deconvolution interferometry, we thus obtain the correct phase, $e^{ik(r_B - r_A)}$, and amplitude, $e^{-\gamma(r_B - r_A)}$, that accounts for the attenuation of the waves that propagate between the two receivers. Note that cross correlation requires the power spectrum of the source signal as well as the source location, as where deconvolution interferometry is independent of the source properties. Because of these properties, we use deconvolved wave forms for our attenuation measurements. Equation 5 is potentially unstable when the reference spectrum $U(r_A, \omega) \ \rightarrow \ 0$. For our method, we use a stabilized deconvolution given by

$$\begin{aligned} D(r_B, r_A, \omega) &= \frac{U(r_B, \omega)}{U(r_A, \omega)} \\ &\Rightarrow \frac{U(r_B, \omega) U^*(r_A, \omega)}{U(r_A, \omega) U^*(r_A, \omega) + \epsilon}, \end{aligned} \tag{3.6}$$

where we take ϵ to be 1% of the average power of $U(r_A, \omega)$.

3.2 Methodology

Attenuation of waves is expressed in the quality factor that is defined as the relative energy loss over a cycle of oscillation (Aki and Richards, 1980). Estimations of attenuation can be made by measuring the loss in the amplitudes as waves propagate between receivers. These estimations are based on the assumptions that both receivers are coupled accurately to the medium, and the amplitude picks correspond to the same seismic event. Previous studies of Snieder and Şafak (2006) measured

attenuation with the Millikan Library data using interferometry to reduce the imprint of a variable receiver coupling. Our method estimates attenuation from individual recordings deconvolved with a common signal, and estimates can be averaged over the array of recordings to reduce and estimate the error. Deconvolution interferometry with a reference signal decomposed into upgoing and downgoing waves, generates wave states with an impulsive upgoing and downgoing wave, respectively, at the base of the building (Snieder et al., 2006). The upgoing and downgoing wave forms of an individual receiver can be compared to give measurements of attenuation.

We separate the wave field at the base of the building into upgoing (u_+) and downgoing (u_-) waves using the following decomposition (Robinson, 1999):

$$\frac{\partial u_+}{\partial t} = \frac{1}{2}\left(\frac{\partial u}{\partial t} - c\frac{\partial u}{\partial z}\right) \tag{3.7}$$

$$\frac{\partial u_-}{\partial t} = \frac{1}{2}\left(\frac{\partial u}{\partial t} + c\frac{\partial u}{\partial z}\right). \tag{3.8}$$

The z-derivative follows from the difference of the motion recorded in the basement and on the first floor. We use the value $c = 322\ m/s$ as determined by Snieder and Şafak (2006).

Deconvolving the wave forms with their upgoing and downgoing waves separates the signal into causal and acausal waves (Snieder et al., 2006). The causal and acausal wave forms would be symmetric in time if attenuation were not present. We measure the attenuation from the differences in the causal and time-reversed acausal wave forms of each floor. The procedure begins by directionally separating the wave fields in the reference floor using equations (7) and (8). We choose the basement floor recording as our reference signal and separate the signal into upgoing and downgoing waves. I estimate the z-derivative from the differences in the motion recorded in the basement and at the first floor. The dip filter described above, generates wave forms that are either causal or acausal in the floors above the basement. This procedure simulates a pure upgoing or downgoing impulsive virtual source in the basement at

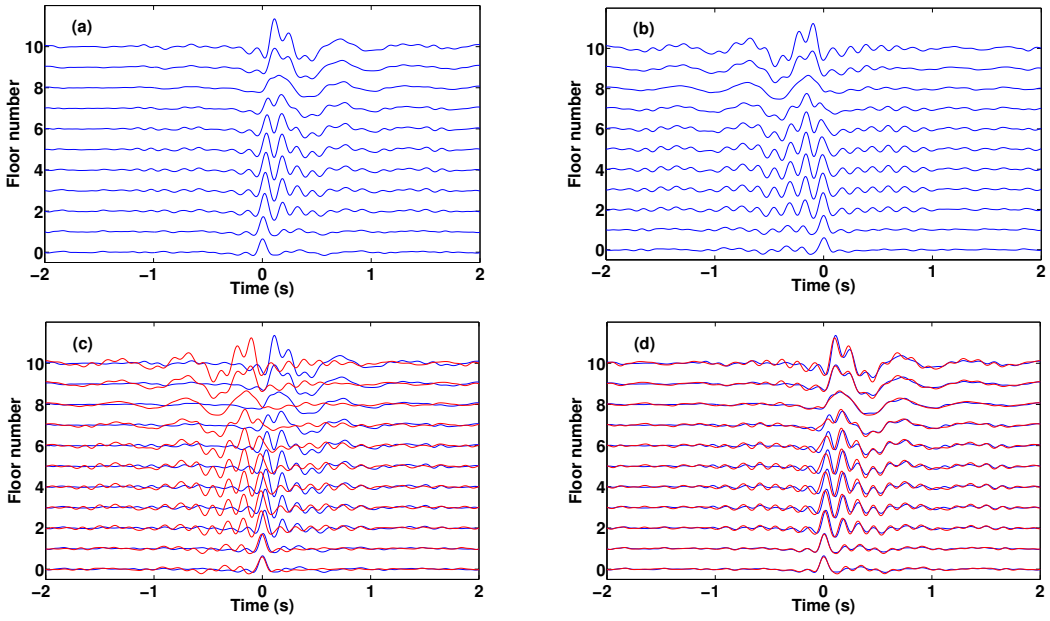

Figure 3.3: Wave forms deconvolved with decomposed waves and their superpositions both before and after time reversal. a) Wave forms obtained by deconvolving the waves at every floor with the upgoing wave in the basement, b) with the downgoing wave in the basement, c) superposition of causal and acausal wave forms of above figures, d) and superposition after time reversal of acausal wave forms.

$t = 0$.

Using only the upgoing waves in the reference signal, our interferometry method extracts the building response from an upgoing impulsive source in the basement of the building at $t = 0$. The deconvolutions of all the floors, in the frequency domain, are ratios of the full wave field spectra of an individual floor and the upgoing wave spectra of the reference floor. We apply this type of deconvolution to all the floors to get eleven deconvolved wave forms (Figure 3.3a). Deconvolution, with the upgoing waves in the reference floor, compresses all the upgoing waves in the basement into one upgoing virtual impulse injected at $t = 0$. The response of the building to this virtual source is non-zero for times $t > 0$. The use of the upgoing waves for deconvolution generates causal wave forms because the building only oscillates after the upgoing wave enters the building. In a similar manner, we also deconvolve the full wave forms of each individual floor with the downgoing wave form from the basement signal. This downgoing wave is the result of upgoing waves entering the building at earlier times (i.e. $t < 0$). This procedure therefore generates acausal wave forms (Figure 3.3b). Collapsing all the downgoing waves in the basement to one downward impulse, requires energy to be present in the building before time $t = 0$, which corresponds to the acausal wave forms seen in Figure 3.3b.

A superposition of the causal and acausal wave forms of Figures 3.3a and 3.3b as shown in Figure 3.3c, reveal a quasi-symmetry of the wave forms around $t = 0$. Time reversal breaks down under certain conditions, such as rotation, flow, and intrinsic attenuation (Fink, 2006). The intrinsic attenuation in the building has broken the time reversal symmetry of the wave forms in Figure 3.3c. This is apparent from Figure 3.3d, where the acausal wave forms generated from the deconvolution using downgoing waves of the reference floor, have been time reversed. This plot shows the superposition of the time reversed acausal wave forms and causal wave forms. Note that the amplitudes do not match, and from this difference in amplitudes we measure

attenuation.

We band-pass filter the deconvolved signals using Butterworth filters of the 3rd and 2nd order to the respective dominant frequency bands 0.2-3.0 Hz and 5.0-7.8 Hz of the power spectra shown in Figure 3.4. This allows us to retrieve constant Q values within each frequency band chosen for analysis, and thereby yielding a frequency-dependent Q in a discrete sense. After band-pass filtering our deconvolved signals using the frequency bands of Figure 3.4, we compute the envelopes of all the wave forms. To demonstrate the estimation of attenuation, we discuss the procedure for the low frequency band-passed data in detail.

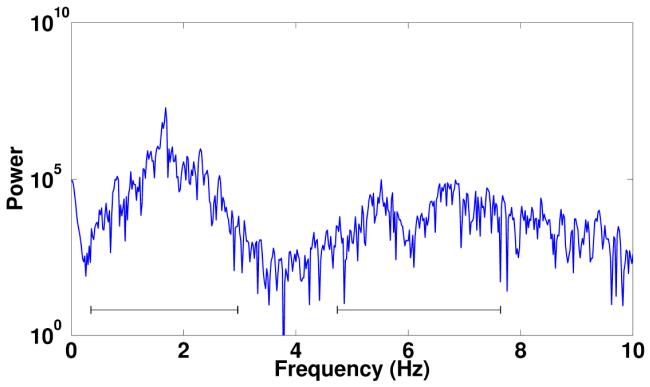

Figure 3.4: The rms power spectra of floor 7 with horizontal bars indicating the frequency bands used for band-pass filtering.

The two curves depicted in Figure 3.5, are a deconvolved wave form from the upgoing wave of floor 4 (gray curve) and the envelope corresponding to this wave form (black curve). This deconvolved wave form is generated from the spectra of the fourth floor and the upgoing wave at the basement. We then apply the low frequency Butterworth band-pass filter of order 3 to this deconvolved wave form. The envelope is acquired from the modulus of the analytic signal using the Hilbert transform. We next take the natural logarithm of this wave form (Figure 3.6). The second curve is

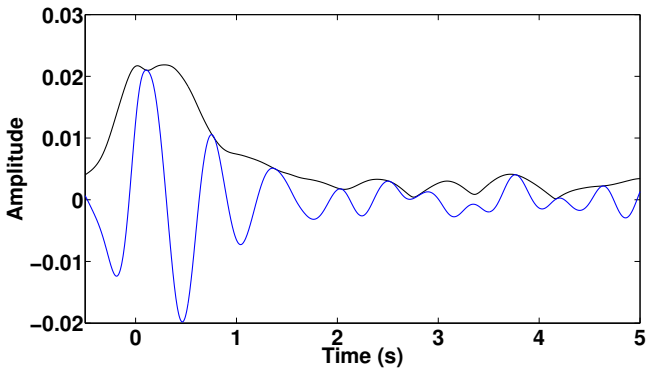

Figure 3.5: Signal from floor 4 deconvolved with upgoing waves after low band-pass filtering (blue curve). Envelope of the corresponding signal (black curve).

the natural logarithm of the envelope of the wave from the fourth floor obtained from deconvolution using the downgoing wave and time reversed.

The first observation is that these two curves are not the same; this difference is due to attenuation. The second observation is that these curves decay almost linearly for the first 2 seconds. During this time duration, the difference of these natural logarithms is also linear with respect to time, and a constant Q value model corresponds to the slope of the difference of these curves. This model is set up by examining the envelopes of the deconvolved signals of an individual floor. We define the envelopes of the deconvolved signals to be

$$\begin{aligned} d_+(t) &= A_+ \, e^{-mt} \\ d_-(-t) &= A_- \, e^{+mt}. \end{aligned} \tag{3.9}$$

Taking the natural logarithm of the ratio of d_+ to d_- yields an equation suited for a linear regression where the slope parameter solves for the attenuation coefficient m in a least-squares sense.

$$\ln \left| \frac{d_+}{d_-} \right| = -2mt \tag{3.10}$$

This model does make the assumption that the initial amplitudes are approximately equal, such that $A_+ \approx A_-$. Figure 3.7, shows the difference of the curves (black curve)

of Figure 3.6, for the initial 2 seconds, and the linear least-squares fit (magenta curve). This procedure is repeated for all the floors, excluding floor 8 because of receiver coupling issues, to generate estimates of the attenuation coefficient.

We also use this procedure for the higher frequency band-pass filtered data of 5.0-7.8 Hz. In this case, the linear trend of the difference of natural logarithms of the envelopes only has a 1 second duration. The higher frequency content of the signal is expected to lead to a more rapid decay of the envelope than of the low frequency content. Figure 3.8 shows that noise dominates the signal after 1 second duration because the envelope stabilizes to a near-constant value after that time. Therefore we do our fitting within the first second, and this fitting of the difference of the curves of Figure 3.8 can be seen in Figure 3.9.

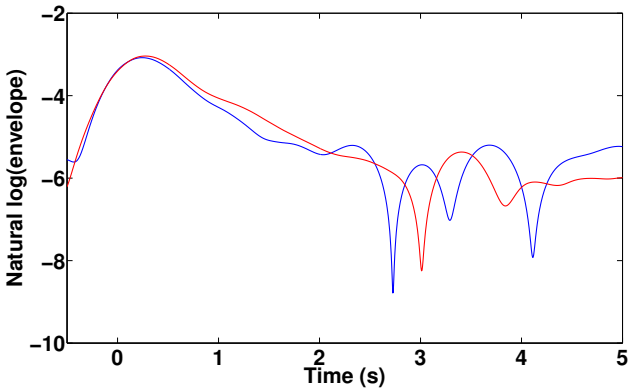

Figure 3.6: The natural log of envelopes from upgoing and downgoing deconvolved wave forms after low frequency 0.2-3.0Hz band-pass filtering

To estimate the error in our measurement of ζ due to errors in the slope of the fitting curve and the width of the employed frequency band, we use the following equations. If we write the attenuation coefficient as

$$m = \bar{\omega}\zeta, \tag{3.11}$$

where $\bar{\omega}$ is the weighted mean of the angular frequency for a given frequency band, and the attenuation coefficient m is given by the slope from our fitting curve, we

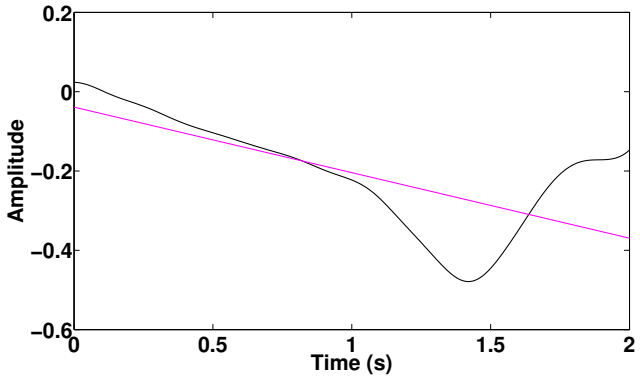

Figure 3.7: The difference of the curves in Figure 3.6 (black curve), and linear fit (magenta curve)

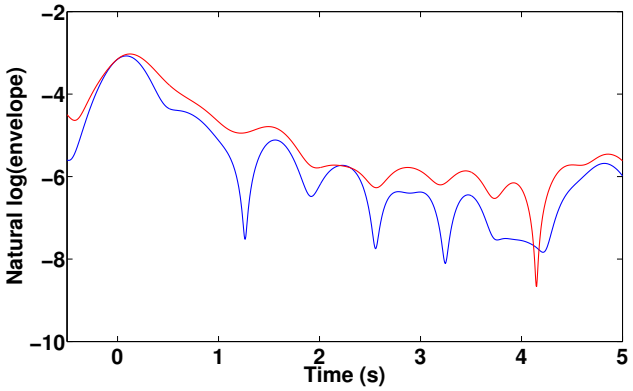

Figure 3.8: The natural log of envelopes from upgoing and downgoing deconvolved wave forms after high frequency 5.0-7.8Hz band pass filtering

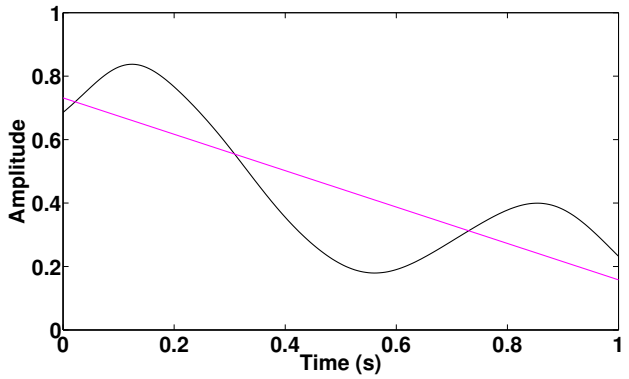

Figure 3.9: The difference of the curves in Figure 3.8 (black curve), and linear fit (magenta curve)

Table 3.1: Damping Coefficients; TR = time reversal, NM = normal mode, TW = traveling wave

Method	ζ	σ_ζ	Frequency Mode
TR	1.14%	0.50%	fundamental
NM	1.15%	0.41%	fundamental
Newton (half-power)	1.57%	NA	fundamental
Bradford et al.	2.39%	NA	fundamental
Clinton et al.	1.63%	NA	fundamental
Kuroiwa (half-power)	1.54%	NA	fundamental
Kuroiwa (mode shape)	1.47%	NA	fundamental
Kuroiwa (Hudson's)	1.74%	NA	fundamental
TR	1.74%	0.39%	first overtone
TW	1.58%	1.36%	first overtone

estimate the error for the i^{th} floor using

$$\sigma_{\zeta,i} = \sqrt{\frac{m_i^2}{\bar{\omega}^2}\left(\frac{\sigma_{m,i}^2}{m_i^2} + \frac{\sigma_\omega^2}{\bar{\omega}^2}\right)}\,, \tag{3.12}$$

where σ_ω is our standard deviation of $\bar{\omega}$ given by

$$\bar{\omega} = \frac{\int_\Omega \omega P(\omega) d\omega}{\int_\Omega P(\omega) d\omega}, \tag{3.13}$$

$$\sigma_\omega^2 = \frac{\int_\Omega (\omega - \bar{\omega})^2 P(\omega) d\omega}{\int_\Omega P(\omega) d\omega}, \tag{3.14}$$

where $P(\omega)$ is the power spectrum within the employed frequency band Ω. $\sigma_{m,i}$ is our standard deviation of the attenuation coefficient of the i^{th} floor from estimates of the discrepancy of the data from the least-squares linear fit (Bevington and Robinson, 2003). This procedure for $\sigma_{\zeta,i}$ is repeated and averaged for all the floors except the eighth floor. Equation (12) is based on the assumption that the frequency and slope are independent measurements, and therefore that their covariance vanishes. The attenuation estimates with their errors are presented in Table 1.

3.3 Relation to Previous Work

The motion of the Millikan Library has been used before to estimate intrinsic attenuation using deconvolution interferometry (Snieder and Şafak, 2006), and we

compare our results to these past measurements. Snieder and Şafak (2006) developed two techniques using deconvolution interferometry. A technique that measures attenuation from the normal mode oscillation of the building and another that measures attenuation from higher frequency traveling waves.

The technique employing the normal mode oscillations of the building uses the basement floor signal as the reference signal for the deconvolution defined by Equation 6. This technique, however, does not decompose the wave field into up and downgoing waves. Using the full spectra of the reference signal, we generate the deconvolution wave forms in Figure 3.10. In this figure, the motion at the basement floor is compressed to a band-limited spike at $t = 0$. For $t > 0$, the figure shows the response of the building to the impulsive excitation. This response is dominated by the fundamental mode of the building with a period of about 0.6 seconds.

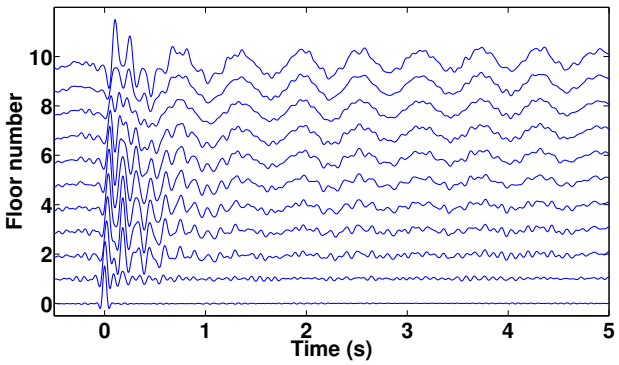

Figure 3.10: The motion of the building in Figure 3.1 after deconvolution with the motion recorded in the basement.

We first bandpass filter the waveforms of Figure 3.10 between 0.2-3.0 Hz, using the low frequency range indicated by the left horizontal bar in Figure 3.4. A linear curve is fit to the natural logarithm of the envelopes of the deconvolved wave forms similar to our time reversal method. Figure 3.11 shows the natural logarithm of the envelope of the signals in Figure 3.10 in solid lines and the least-squares fits in dashed lines. The slope of the least-squares fits is proportional to the attenuation coefficient. Table 1 shows the average damping estimate corresponding to the normal mode measurement

indicated NM for this method. An attempt to measure the damping with this method at the higher frequency band yielded poor results. This is due to low amplitude in the power spectrum of the frequency band of 5.0-7.8 Hz.

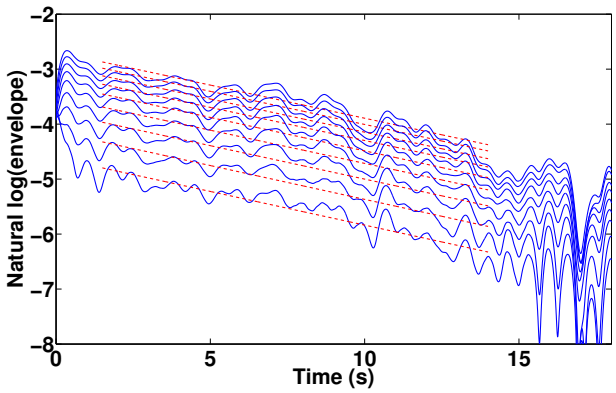

Figure 3.11: Natural log of envelopes from signals in Figure 3.10 (solid curves), and linear fit (dashed curves)

The next deconvolution interferometry technique developed by Snieder and Şafak (2006) uses higher frequency traveling waves. Snieder and Şafak (2006) make their attenuation measurements using the top floor signal as the reference signal for the deconvolution. Note that there is no decomposition of the wave fields at the reference floor for this traveling wave procedure. The deconvolved wave forms in Figure 3.12 uses the full spectra of each signal. In Figure 3.12, a traveling wave moves up and then down the building. Knowing the shear velocity of the building, the ratio of the amplitudes of the upgoing and downgoing waves, the distance traveled from each receiver to the top of the building and back down to the receiver, and the travel times, one can estimate the attenuation. Table 1 displays the results of these measurements marked TW for the traveling wave technique. Since this estimate depends only on the amplitude ratio of the upgoing and downgoing waves at each floor, this estimate is not affected by variations in receiver coupling. The observation that the signals are quiescent after the traveling wave has moved up and down through the building in Figure 3.12 also suggests there is little scattering caused by the individual floors.

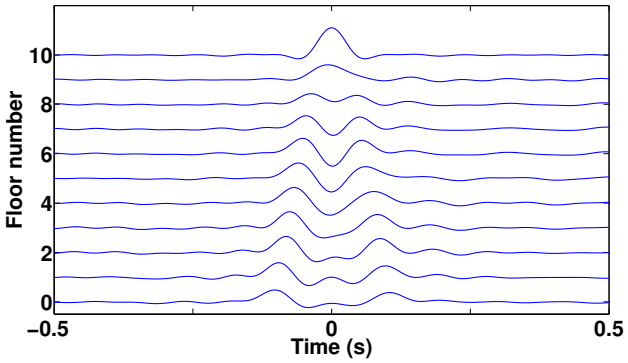

Figure 3.12: The motion of the building in Figure 3.1 after deconvolution with the motion at the top floor.

3.4 Discussion

Table 1 shows that our method of using deconvolution interferometry with time reversal gives estimates of attenuation that compare well to values found previously using seismic interferometry and classical methods. The new method we propose has several benefits compared to the past methods. Our method recovers attenuation estimates in the normal mode and the first overtone. This makes the new proposed method more robust than the past interferometric methods because the proposed method's ability to perform at higher frequencies. Classical methods, such as the half-power method, lose their robustness in higher overtones because of uncertainty in the half-power amplitude picks on either side of the peak frequency for a given overtone.

This method removes the radiation damping from the global attenuation estimate, leaving only internal mechanisms for energy loss like scattering attenuation, constant Coulomb internal friction, and intrinsic material attenuation. This proposed method shares the ability to separate the radiation damping with past seismic interferometric methods. Table 1 gives estimates that employ classical modal analysis that are available in the literature (Bradford et al., 2004; Clinton et al., 2006; Kuroiwa, 1967). These methods recover global damping values of the soil-structure system. These val-

ues include radiation damping that occurs at the soil-structure interface. Our method using deconvolution interferometry with time reversal removes the radiation damping by allowing the energy to leave the system. For instance, the upgoing deconvolution used in our proposed method simulates one upgoing wave injected into the building in the basement at time $t = 0$. The wave moves up and then down through the building and continues down. In essence there is a reflection coefficient of 0 in the basement. This leaves only internal mechanisms of attenuation in our deconvolved signals from which we measure. Figure 3.12, of the traveling wave experiment, indicates that there may be little contribution from scattering attenuation. Combining classical methods with our proposed method could refine our knowledge of civil structure behavior and improve earthquake modeling.

Our method is built upon a linear mathematical framework which may lead to limitations in this method and require an attenuation model representation beyond the constant Q description. This method is described by a linear elastic behavior of the medium, and strong shaking may invalidate the assumption of linearity. Structures proximal to epicenters of large earthquakes will have strong ground motion excitation which can generate nonlinear effects due because the mechanical properties of the building may depend on excitation levels (Clinton et al., 2006). In this dataset for the Millikan Library we did not observe many internal reflections and consequently little scattering attenuation. Datasets with stronger scattering attenuation may introduce complications to this method's ability to accurately measure intrinsic attenuation.

In the future, this method should be tested on more data to further understand the limitations of this method. Elements of nonlinearity and other sources of attenuation could pose problems for this method. Other civil structures with different geometries such as other building designs, bridges, and downhole arrays could also benefit from this method of attenuation investigation. An extension to include higher degrees of freedom would benefit this method to perform in more complex structures. This new

method of deconvolution interferometry with time reversal has proved to be a viable method for this dataset and should be continued to be explored for further advanced applications.

3.5 Conclusion

We have shown using data recorded in the Millikan Library that deconvolution interferometry with time reversal is an effective method to measure attenuation in civil structures. This method extracts estimates of intrinsic attenuation from the breaking of time reversal symmetry. By time reversing the acausal wave forms, we estimate intrinsic attenuation using a fitting procedure that is similar to past methods using normal mode oscillations. By comparing the estimates of our time reversal method to that of past seismic interferometry methods, we have shown that our results compare well to the past methods of Snieder and Şafak (2006). Additionally, the time reversal method has higher precision than the traveling wave method and not constrained to measuring only the fundamental mode.

3.6 Data and Resources

The data are recorded and made available through the National Strong Motion Project Data Sets of the US Geological Survey. The data for the Yorba Linda earthquake can be accessed through:
`http://nsmp.wr.usgs.gov/data_sets/20020903_1.html#Downloads`

CHAPTER 4
GABOR DECONVOLUTION

In the previous chapter, I presented a method using deconvolution interferometry and time reversal to measure intrinsic attenuation in a civil structure aligned with a vertical array of accelerometers. This method provided attenuation estimates for the normal and first higher mode of oscillation of the Millikan Library. The fitting procedure was done in the time domain.

Gabor (1946) presented the concepts of time-frequency analysis on communication signals. Typical signal analysis takes place in either the time or frequency domain, but Gabor suggests a time-frequency domain analysis because "time and frequency play symmetrical parts." His work discusses the precision limitations that are consequences of sampling time signals for time-frequency analysis. The product of the uncertainty in time and frequency of any time signal obeys a lower bound. Therefore, a suitable time duration of the signal should be chosen for analysis to complement a suitable bandwidth for a given measurement.

4.1 Theory and Methodology

Theoretically, we should be able to optimize the error in both the time and frequency domain, with regard to the Gabor limit, when estimating attenuation by using Gabor deconvolution. Gabor deconvolution operates in the time-frequency domain by windowing segments of the time signal and Fourier transforming these segments. Each windowed segment overlaps the adjacent segment by a percentage which is typically larger than fifty percent. The analysis lies in the realm of short-time Fourier transforms which is analogous to Gabor transforms when a Gaussian is chosen for the

windowing function. Grossman et al. (2001) defines the Gabor transform, V_g to be

$$V_g s\left(\tau,\omega\right)=\int_{-\infty}^{\infty} s\left(t\right) g\left(t-\tau\right) e^{-i\omega t} dt. \tag{4.1}$$

The time signal $s(t)$ is windowed by the Gabor analysis window $g(t)$, which is typically a Gaussian or a raised cosine window such as a Hann or Hamming window. The Gabor analysis window $g(t)$ slides through the time signal $s(t)$ with the center of the Gabor analysis window falling on the time sample τ. At each position of the Gabor analysis window a Fourier transform is made.

The time signal, $s(t)$ is considered to be nonstationary and is represented to be Grossman et al. (2001); Margrave (1998); Margrave et al. (2002)

$$S\left(\omega\right)=W\left(\omega\right)\int_{-\infty}^{\infty}\alpha\left(t,\omega\right) r\left(t\right) e^{-i\omega t} dt. \tag{4.2}$$

The source wavelet spectrum $W(\omega)$ is stationary in time and convolved with the attenuation operator $\alpha(t,\omega)$ and reflection series $r(t)$. This description of the nonstationary time signal $s(t)$ is transformed into a mix domain by the Gabor transform (Grossman et al., 2001). The absolute value of the transformed nonstationary signal has, in the frequency domain, the form:

$$\left|V_g s\left(\tau,\omega\right)\right|=\left|W\left(\omega\right)\right|\left|\alpha\left(\tau,\omega\right)\right|\left|V_g r\left(\tau,\omega\right)\right| \tag{4.3}$$

$$\left|V_g s\left(\tau,\omega\right)\right|\approx\left|W\left(\omega\right)\right|\left|\alpha\left(\tau,\omega\right)\right|. \tag{4.4}$$

Following the assumption of Grossman et al. (2001), the Gabor transformed reflectivity series $V_g r(t)$ can be assumed to have a "white" spectrum and thus average to unity. This assumption is valid because deconvolution interferometry simulates a boundary condition where the reference signal fully reflects energy without changing the wave state (Snieder et al., 2006). With this assumption, equation 4.3 simplifies to equation 4.4. The authors continue by generating a least-squares problem to minimize α for Q by assuming $|\alpha(\tau,\omega)|=e^{-\omega\tau/2Q}$, or equivalently $ln|\alpha|+\omega\tau/2Q=0$. Inserting equation 4.3 for $|\alpha|$ and minimizing the result in the least-squares sense

leads to the objective function

$$\Phi\left(Q,W\right)=\int_{\Omega}\left(ln\frac{V_{g}s\left(\tau,\omega\right)}{W\left(\omega\right)}+\frac{\omega\tau}{2Q}\right)^{2}d\tau d\omega. \tag{4.5}$$

Where Ω is the appropriate time duration and bandwidth under investigation. Evaluating equation 4.5 and solving for Q, Grossman et al. (2001) find

$$Q=\pi\frac{\int_{\Omega}\tau^{2}f^{2}\ \ d\tau df}{\int_{\Omega}\tau f\ \ ln\frac{W\left(f\right)}{V_{g}s\left(\tau,f\right)}\ \ d\tau df}. \tag{4.6}$$

Where $f=\omega/2\pi$ is the frequency in Hertz.

Grossman et al. (2001) continue solving for Q by assuming a source wavelet spectrum $W(f)$. Assuming a source wavelet is a risky task when the source is not determined. With seismic interferometry the source spectrum is known because it is redatumed to a known receiver location.

Equation 4.6 can be extended by using signals generated from deconvolution interferometry and time reversal. In Chapter 3, deconvolution interferometry was applied to the Millikan Library time signals after separating wave fields into upgoing and downgoing waves. I can continue to work with these deconvolved signals and Gabor transform them into:

$$\begin{aligned} V_{g}d_{+}\left(\tau,f\right) &= W_{+}\left(f\right)e^{\frac{-\pi f\tau}{Q}} \\ V_{g}d_{-}\left(\tau,f\right) &= W_{-}\left(f\right)e^{\frac{\pi f\tau}{Q}} \end{aligned}$$

If we consider $W_{+}\approx W_{-}$, then the ratio $V_{g}d_{-}/V_{g}d_{+}=e^{\frac{2\pi f\tau}{Q}}$, and taking the natural logarithm, the ratio becomes $ln|V_{g}d_{-}/V_{g}d_{+}|=2\pi f\tau/Q$. Substituting the natural logarithm of the ratio above into equation 4.6 and multiplying by a factor of 2 to acquire Q estimate such that equation 4.6 becomes

$$Q=2\pi\frac{\int_{\Omega}\tau^{2}f^{2}\ \ d\tau df}{\int_{\Omega}\tau f\ \ ln\frac{V_{g}d_{-}\left(\tau,f\right)}{V_{g}d_{+}\left(\tau,f\right)}\ \ d\tau df}. \tag{4.7}$$

Table 4.1: Damping Coefficients; TR = time reversal, NM = normal mode, TW = traveling wave, GTR = Gabor time reversal

Method	ζ	σ_ζ	Frequency Mode
TR	1.14%	0.50%	fundamental
NM	1.15%	0.41%	fundamental
GTR	1.59%	NA	fundamental
TR	1.74%	0.39%	first overtone
TW	1.58%	1.36%	first overtone
GTR	0.23%	NA	first overtone

Theoretically, this should give accurate values of Q. In practice, the results for the normal frequency mode were comparable to previous esitmates, but not the estimate for the first higher mode. No error analysis was done on the Gabor method because the priority was getting measurements comparable to previous methods.

4.2 Results

Equation 4.7 gives Q estimates for deconvolution interferometry signals with time reversal, but the results were not comparable. I have applied this method to the Millikan Library data with results that agree with estimates for the normal mode frequency band, but with inaccurate results for the higher frequency band.

I implement equation 4.7 by defining Ω to include only the frequency band of 0.2-3.0 Hz for the normal mode and Ω to include only 5.0-7.8 Hz for the first higher mode. The results of the Gabor method labeled GTR are presented in Table 4.1. For comparison, previous methods using deconvolution interferometry to acquire attenuation estimates are expressed in the damping ratio ζ.

Table 4.1 show that the attenuation coefficients obtained by the Gabor deconvolution for the fundamental mode agree well with estimates obtained from other methods within the observational errors. For the first overtone, there are discrepancies between the attenuation estimates obtained from Gabor deconvolution, and other methods. It is not well understood why the Gabor deconvolution cannot ac-

quire accurate attenuation estimates. The inaccuracy in my Q measurement of the first overtone most likely is related to the ratio of the Gabor transformed deconvolved signals in equation 4.7.

CHAPTER 5
CONCLUSION

Geophysics continues to be a science that investigates Earth by using observed seismic waves. By injecting energy into the Earth, we introduce wave fields whose propagation characteristics depend on material properties in the Earth. The important properties of time reversal symmetry and intrinsic attenuation are inherently a part of wave propagation. Because attenuation in the Earth is generally weak ($Q \approx 100$), we assume, in practice, that TR invariance and attenuation are mutually exclusive.

TR is a valuable property to back-project seismic or ground penetrating radar (GPR) data on reflecting surfaces as part of the imaging process. This renders seismic and GPR images comprised of subsurface velocities and densities and electrical permittivities, respectively, with depth. TR symmetry is broken in the presence of intrinsic attenuation, flow in the medium, and/or rotations of the medium. This thesis focused on intrinsic attenuation affecting the TR symmetry of geophysical data.

Intrinsic attenuation affects the amplitude of geophysical data through effects on the amplitude of wave fields. This allows imaging algorithms to acquire the correct kinematics and have amplitudes stack out images with strong reflectors through constructive interference. Of course, if the attenuation is strong, the amplitudes do not stack out. This explains why gaining procedures are done to enhance the imaging process.

TR applied to geophysical data can also indicate the presence of attenuation by discrepancies in the amplitudes of causal and time reversed acausal signals. By applying a dip filter to the Millikan data to decompose observed waves into upgoing and downgoing wave fields, I generated impulse response functions from an upgoing

and downgoing source and compared their quasi-symmetrical time signals. I utilized the breaking of TR symmetry to diagnose the presence of intrinsic attenuation in the Millikan Library by reversing the acausal signals into causal signals. This provided observations that the signals were asymmetric due to differences in their amplitudes. A linear least-squares fitting procedure was designed to optimize for attenuation for different frequency modes in the building.

This method introduced a new way to measure the intrinsic attenuation of a building fitted with seismic recording instruments that has been subjected to ground motion from earthquakes and active sources. The method was only possible through deconvolution interferometry which yields the impulse response function to a virtual shear source excited in the basement of the building at time $t = 0$. The fitting procedure was done in the time domain which allowed for intrinsic attenuation estimates for two frequency bands representing the fundamental and first higher mode. This is an advance in building monitoring compared to previous methods that include half-power, mode shape, and Hudson's methods for acquiring attenuation estimates because with these methods only the attenuation associated with the fundamental mode could be found. Though this method of deconvolution interferometry and time reversal has worked for the Yorba Linda earthquake data taken from the Millikan Library, other data sets should be tested for robustness with this proposed method.

This method estimated intrinsic attenuation measurements in the time domain through a linear least-squares fitting procedure. This brings up the uncertainty principle in which the uncertainty in the time domain is inversely proportional to the uncertainty in the frequency domain. If we decrease our uncertainty in the frequency domain then we increase our uncertainty in the time domain.

The Gabor method discussed in Chapter 4 has potential to acquire accurate estimates of attenuation, but more effort needs to be given in discovering error sources and optimizing frequency and time samples to optimize resolution.

5.1 Future work

The deconvolution interferometry method with time reversal should be tested on more data sets of civil structures to test for robustness. Testing for robustness should include buildings with different geometries that could prove challenging for this method. The Millikan Library has a geometry that is simple and closely resembles a clamped a beam. There are data sets for buildings much different than the Millikan Library, with respect to geometry, that are fitted with seismic receivers that could provide interesting results from the application of the proposed method of deconvolution interferometry with time reversal.

Civil structures such as bridges should also be tested to see if there is an application to these structures. Though bridges would require a horizontal array, this should not compromise the accuracy of this proposed method.

Borehole data could also be ideal for acquiring attenuation estimates for deconvolution interferometry with TR. The geometry of seismic arrays in a borehole, such as vertical seismic profiles (VSP), are well designed for this method. The benefit to applying this method to VSP data is that the source used in VSP lies in the surface seismic frequency band. Many times acoustic sonic logs are used to acquired Q estimates, but these sources are several orders of magnitude greater than surface seismic sources. Acoustic sonic logs should not be dismissed either. The application of my method could also be beneficial to acquiring attenuation estimates for acoustic sonic logs as well.

Lastly, the Gabor method should be further investigated to better understand its potential to yield accurate estimates of attenuation. Applying the Gabor deconvolution to the Millikan Library data set has been inconclusive on whether it is a viable method for attenuation estimation. Error analysis should be performed to understand where there are significant contributions of error. More studies should be conducted with Gabor deconvolution to include attenuation estimates of higher modes.

REFERENCES CITED

Aki, K., and P. G. Richards, 1980, Quantitative seismology : Theory and methods: W. H. Freeman, San Francisco.

Anderson, B.E., Griffa, M., Larmat, C., Ulrich, T.J., and Johnson, P.A., 2008, Time Reversal: Acoustics Today, **4**(1), 5-16.

Anderson, B.E., Griffa, M., Larmat, C., Ulrich, T.J., and Johnson, P.A., 2011, Time reversal reconstruction of finite sized sources in elastic media: J. Acoust. Soc. Am., **130**, EL219-EL225.

Bakulin, A., and R. Calvert, 2006, The virtual source method: Theory and case study: Geophysics, **71**, SI139–SI150.

Bakulin, A., A. Mateeva, K. Mehta, P. Jorgensen, J. Ferrandis, I. S. Herhold, and J. Lopez, 2007, Virtual source applications to imaging and reservoir monitoring: The Leading Edge, **26**, 732–740.

Batzle, M., Hoffman, R., Prasad, M., Kumar, G., Duranti, L., and Han, D., 2005, Seismic attenuation: observations and mechanisms: 75th Annual International Meeting, SEG, Expanded Abstracts, 1565-1569.

Behura, J., Batzle, M., Hoffman, R., and Dorgan, J., 2007, Heavy oils: Their shear story: Geophysics, **72**, 175-183.

Bevington, P., and D. Robinson, 2003, Data reduction and error analysis for the physical sciences: McGraw-Hill. McGraw-Hill Higher Education.

Bradford, S.C., J.F. Clinton, J. Favela, and T.H. Heaton, 2004, Results of Millikan Library forced vibration testing: Technical Report, California Institute of Technology, http://resolver.caltech.edu/Caltech- EERL:EERL-2004-03 (last accessed March 2012).

Calvert, R. W., 2003, Seismic imaging a subsurface formation: U.S. Patent 20030076740.

Carder, D. S., 1936, Observed vibrations of buildings: Bull. Seismol. Soc. Am., **26**, 245-277.

Çelebi, M., L. T. Phan, and R. D. Marshall, 1993, Dynamic characteristics of five tall buildings during strong and low-amplitude motions: The Structural Design of Tall Buildings, **2**, 1-15.

Chopra, A. K., and F. Naeim, 2007, Dynamics of structures—theory and applications to earthquake engineering, third edition: Earthquake Engineering Institute of America, Berkley, California.

Claerbout, J.F., 1971, Toward a unified theory of reflector mapping: Geophysics, **36**, 467-481.

Clinton, J. F., S. C. Bradford, T. H. Heaton, and J. Favela, 2006, The observed wander of the natural frequencies in a structure: Bull. Seismol. Soc. Am., **96**, 237-257.

Constable, S. and Srnka, L.J., 2007, An introduction to marine controlled-source electromagnetic methods for hydrocarbon exploration: Geophysics, **72**, 3-12.

Curtis, A., P. Gerstoft, H. Sato, R. Snieder, and K. Wapenaar, 2006, Seismic interferometry–turning noise into signal: The Leading Edge, **25**, 1082–1092.

Dasgupta, R. and Clark, R., 1998, Estimation of Q from surface seismic reflection data: Geophysics, **63**, 2120-2128.

Derode, A., Roux, P., and Fink, M., 1995, Robust acoustic time reversal with high-order multiple scattering: Phys. Rev. Let., **75**, 4205-4210.

Derode, A., E. Larose, M. Campillo, and M. Fink, 2003, How to estimate the Green's function of a heterogeneous medium between two passive sensors? Application to acoustic waves: Appl. Phys. Lett., **83**, 3054-3056.

Fink, M., 2006, Time-reversal acoustics in complex environments: Geophysics, **71**, SI151–SI164.

Foutch, D.A., 1976, A study of the vibrational characteristics of two multistory buildings, *Ph.D. Thesis*, California Institute of Technology, Earthquake Engineering Research Laboratory, Pasadena, California.

Futterman, W.I., 1962, Dispersive body waves: J. Geophys. Res., **67** 5279-5291.

Gabor, D., 1946, Theory of communication. Part 1: The analysis of information: The Journal of the Institute of Electrical Engineers-Part III: Radio and Communication Engineering, **93**, 429-441.

Gautam, K., 2003, Fluid effects on attenuation and dispersion of elastic waves: *Ph.D. Thesis*, Colorado School of Mines, Golden, Colorado.

Gosselet, A., and S. C. Singh, 2007, Using symmetry breaking in time-reversal mirror for attenuation determination: SEG Technical Program Expanded Abstracts, **26**, 1639–1643.

Grossman, J.P., Margrave, G.F., Lamoureux, M.P., and Aggarwala, R., 2001, Constant-Q estimation via a nonstationary Gabor spectral model: CREWES Research Report, **17**.

Halliday, D., and A. Curtis, 2010, An interferometric theory of source-receiver scattering and imaging: Geophysics, **75**, SA95–SA103.

Kohler, M. D., and T. H. Heaton, 2007, A time-reversed reciprocal method for detecting high-frequency events in civil structures: AGU Fall Meeting Abstracts, B1265–1272.

Kohler, M. D., T. H. Heaton, and S. C. Bradford, 2007, Propagating waves in the steel, moment-frame Factor Building recorded during earthquakes: Bull. Seismol. Soc. Am., **97**, 1334–1345.

Kuroiwa, J., 1967, Vibration tests of a multistory building, *Ph.D. Thesis*, California Institute of Technology, Earthquake Engineering Research Laboratory, Pasadena, California.

Larose, E., L. Margerin, A. Derode, B. van Tiggelen, M. Campillo, N. Shapiro, A. Paul, L. Stehly, and M. Tanter, 2006, Correlation of random wavefields: An interdisciplinary review: Geophysics, **71**, SI11–SI21.

Margrave, G.F., 1998, Theory of nonstationary linear filtering in the Fourier domain with application to time-variant filtering: Geophysics, **63**, 244-259.

Margrave, G.F., Lamoureux, M.P., Grossman, J.P., and Iliescu, V., 2002, Gabor deconvolution of seismic data for source waveform and Q correction: 72nd Annual International Meeting, SEG, Expanded Abstracts, 2190-2193.

Margrave, G.F., Lamoureux, M.P., and Henley, D.C., 2011, Gabor deconvolution: Estimating reflectivity by nonstationary deconvolution of seismic data: Geophysics, **76**, W15-W30.

Minato, S., T. Matsuoka, T. Tsuji, D. Draganov, J. Hunziker, and K. Wapenaar, 2011, Seismic interferometry using multidimensional deconvolution and cross correlation for crosswell seismic reflection data without borehole sources: Geophysics, **76**, SA19–SA34.

Nunez, I and Negreira, C., 2004, Efficiency parameters in time reversal acoustics: Applications to dispersive media and multimode wave propagation: J. Acoust. Soc. Am., **117**(3), 1202-1209.

Prieto, G. A., J. F. Lawrence, A. I. Chung, and M. D. Kohler, 2010, Impulse response of civil structures from ambient noise analysis: Bull. Seismol. Soc. Am., **100**, 2322–2328.

Robinson, E., 1999, Seismic inversion and deconvolution, *in* Handbook of Geophysical Exploration, 4B: Pergamon.

Ruigrok, E., Draganov, D., and Wapenaar, K., 2008, Global-scale seismic interferometry: theory and numerical examples: Geophysical Prospecting, **56**, 395-417.

Schuster, G.T., 2009, Seismic interferometry: Cambridge University Press, Cambridge.

Snieder, R., 2007, Extracting the Green's function of attenuating heterogeneous acoustic media from uncorrelated waves: J. Acoust. Soc. Am., **121**, 2637–2643.

Snieder, R., and E. Şafak, 2006, Extracting the building response using seismic interferometry: Theory and application to the Millikan Library in Pasadena, California: Bull. Seismol. Soc. Am., **96**, 586–598.

Snieder, R., J. Sheiman, and R. Calvert, 2006, Equivalence of the virtual-source method and wave-field deconvolution in seismic interferometry: Phys. Rev. E, **73**, 066620.

Şafak, E., 1999, Wave-propagation formulation of seismic response of multistory buildings: J. Struct. Eng., **125**, 426-437.

Spencer, J.W., Jr., 1979, Bulk and shear attenuation in Berea sandstone: The effects of pore fluids: J. Geophys. Rev., **84**, 7521-7523.

Tarantola, A., 2005, Inverse Problem Theory and Methods for Model Parameter Estimation: SIAM, Philadelphia.

Telford, W.M., Geldart, L.P., and Sheriff, R.E., 1976, Applied Geophysics: Cambridge University Press, London.

Todorovska, M., 2009, Soil-structure system identification of Millikan Library north-south response during four earthquakes (1970-2002); what caused the observed wandering of the system frequencies?: Bull. Seismol. Soc. Am., **99(2A)**, 626-635.

Trifunac, M.D., 1972, Comparisons between ambient and forced vibration experiments, *Earthquake Eng. Struct. Dyn.* **1**, 133-150.

Vasconcelos, I., and R. Snieder, 2008, Interferometry by deconvolution, part 1—theory for acoustic waves and numerical examples: Geophysics, **73**, S115–S128.

Wapenaar, K., D. Draganov, R. Snieder, X. Campman, and A. Verdel, 2010, Tutorial on seismic interferometry: Part 1 — basic principles and applications: Geophysics, **75**, 75A195–75A209.

Winkler, K.W. and Nur, A., 1979, Pore fluids and seismic attenuation in rocks: Geophys. Res. Let., **6**, 1-4.

Winkler, K.W., Nur, A., and Gladwin, M., 1979, Friction and seismic attenuation in rocks: Nature, **277**, 528-531.

Winkler, K.W. and Nur, A., 1982, Seismic attenuation: Effects of pore fluids and frictional-sliding: Geophysics, **47**, 1-15.

Wylie, M.J., Gardner, G.F., and Gregory, A.R., 1962, Studies of elastic wave attenuation in porous media: Geophysics, **27**, 569-589.